



**HAL**  
open science

## **Kinetics of the bcc to hcp phase transition in [ 001 ] -oriented single crystal iron under ramp compression**

M.A. Nassirou Hassan, Nourou Amadou, A. Moussa Hassane, A. Batouré, I.  
Adamou, Thibaut de Rességuier

► **To cite this version:**

M.A. Nassirou Hassan, Nourou Amadou, A. Moussa Hassane, A. Batouré, I. Adamou, et al.. Kinetics of the bcc to hcp phase transition in [ 001 ] -oriented single crystal iron under ramp compression. Computational Condensed Matter, 2024, 41, pp.e00965. 10.1016/j.cocom.2024.e00965 . hal-04788409

**HAL Id: hal-04788409**

**<https://hal.science/hal-04788409v1>**

Submitted on 18 Nov 2024

**HAL** is a multi-disciplinary open access archive for the deposit and dissemination of scientific research documents, whether they are published or not. The documents may come from teaching and research institutions in France or abroad, or from public or private research centers.

L'archive ouverte pluridisciplinaire **HAL**, est destinée au dépôt et à la diffusion de documents scientifiques de niveau recherche, publiés ou non, émanant des établissements d'enseignement et de recherche français ou étrangers, des laboratoires publics ou privés.

## **Kinetics of the bcc to hcp phase transition in [001]-oriented single crystal iron under ramp compression**

M.A. Nassirou Hassan<sup>1</sup>, N. Amadou<sup>1,\*</sup>, A. Moussa Hassane<sup>1</sup>, A. Batouré<sup>1</sup>, I. Adamou<sup>1</sup>, and T. de Rességuier<sup>2</sup>

<sup>1</sup> Département de Physique, Université Abdou Moumouni de Niamey, BP. 10662 Niamey, Niger

<sup>2</sup> Institut Pprime, CNRS, ENSMA, Université de Poitiers, Poitiers, France

### **Abstract**

Non-Equilibrium Molecular Dynamics simulations have been used to investigate the kinetics of the bcc to hcp phase transition in ramp-compressed [001]-oriented single crystal iron in the presence of defects consisting in micro-voids. Depending on the ramp maximum pressure, the microstructure of the daughter hcp phase is observed to be strongly affected by the plastic activity in the parent bcc phase. The hcp phase is first nucleated around the pre-existing microvoids, then it grows along preferential crystal directions and the subsequent volume reduction induces a local relaxation of the pressure. The velocity of the bcc-hcp phase boundary is shown to increase gradually with maximum pressure up to supersonic values. For high over-compression beyond the transition onset pressure, the phase transformation becomes almost instantaneous and essentially independent of the initial defects. Meanwhile, the ramp wave steepens with propagation distance and evolves into a shock front, up to the over-driven regime classically observed in both experiments and hydrodynamic, macro-scale simulations.

keywords: ramp compression, shock wave, Molecular Dynamics, phase transition, plasticity, iron, twinning.

## **1 Introduction**

There is a growing interest in understanding the properties of solid materials under extreme conditions of pressure and deformation induced by dynamic compression. Large scale Molecular Dynamics (MD) simulations play a crucial role as they provide valuable insights into the underlying microprocess at the atomic level. In particular, iron has been extensively studied under shock compression with a focus on the microprocess governing plastic deformation and the dynamics of the structural bcc to hcp phase transformation.

Depending on the atomic interaction model used, various aspects of iron dynamic behavior have been explicated (predicted) in reasonable agreement with experiment. Thus, using the Voter-Chen interatomic potential [1], Kadau et al., have investigated the response to shock compression of both single crystal[2, 3] and polycrystalline iron [4]. The structural bcc to hcp phase transition was observed at around 15 GPa, in good agreement with experiment [5], with only a weak dependence on the direction of shock propagation with respect to crystal orientation. The crystallographic relationships between the parent and product phases are common for martensitic transformations while the developing microstructure has been observed to be orientation-dependent, with both [110] and [111] directions exhibiting a sizable fraction of atoms belonging to the fcc phase not confirmed experimentally to date. Using the same interatomic potential, Shao et al., have investigated the dynamics of the bcc to hcp/fcc structural transition in single crystal iron under ramp compression [6]. It was found that when compressed along the [001] direction, the microstructure of the hcp phase tends to form

---

\*corresponding author: [nourou.amadou@ensma.fr](mailto:nourou.amadou@ensma.fr)

lamellar twins along the (100) or (010) planes. Furthermore, when compressed along the [011] and [111] directions, the microstructure in product phase is much finer than that observed along the [001] direction, because more equivalent {011} planes are activated. Since this early potential was merely fitted to the general Rose et al. equation of state [7], no evidence of plastic deformation before the phase transformation was [predicted](#) in both polycrystal nor single crystal (with or without defects) [2, 3, 4, 8]. This contrasts with the results reported by Wang et al. using a more recent modified analytic embedded-atom-model [9]. Here, in a single crystal shock-compressed along its [001] direction, plastic deformation was observed at around 17 GPa, mediated by dislocation nucleation, propagation and multiplication, before the onset of the structural phase transition which occurs at pressures of 18.0, 22.3, and 23.8 GPa along the [001], [110] and [111] directions, respectively [9]. On the other hand, polycrystalline iron was found to yield around 8-9 GPa, prior to the structural phase transformation around 10-13 GPa depending on the shock strength. In this case, the plastic deformation was mainly dominated by grain boundaries activities and intragranular processes such as dislocation slip. This plastic activity was found to contribute to the phase transition by two different coupling modes resulting in two different variants of transition products [10]. In the same period, Gunkelmann et al., using the modified version of the Ackland potential [11], have reported dislocation-mediated plastic deformation in polycrystalline iron at a pressure of about 10 GPa under shock compression [12]. This plastic deformation was accompanied by a significant 3D relaxation under ramp compression with a long rise time [13], where the structural bcc to hcp phase transition was observed at around 23 GPa.

Later on, using the same Ackland potential [11], Amadou et al. analyzed the coupling between the plastic deformation and the structural bcc to hcp phase transition in single crystal iron [14, 15, 16, 17]. This coupling process is particularly important when single-crystal iron is thermalized to 50 K then compressed along the [001] direction. Ramp compression above the yield strength was shown to produce plastic deformation in the form of twins, then, further compression was observed to induce a hardening-like behavior, where the twins previously formed were progressively removed while no dislocation activity was detected, leading to a strong increase of the shear stress. Such post-yield stiffening of the bcc matrix was shown to inhibit the nucleation of the hcp phase, so that the onset of the phase transformation was shifted to very high pressures (on the order of 100 GPa). For the phase transition to be activated at moderate pressure, one must either let the ramp wave steepen during its propagation to evolve into a shock wave or introduce pre-existing defects such as microvoids within the sample. This remarkable effect speculated by Remington et al. [18] and never reported before, deserves extensive study because it may contribute to the strong variations in the transition onset pressure with the loading rate classically observed experimentally.

Here, we report on the kinetics of the bcc to hcp phase transition when it is activated at moderate pressure in the presence of defects and on the coupling between this transition and wave propagation.

## 2 Method and computational details

Non-Equilibrium Molecular Dynamics (NEMD) simulations have been used to investigate the kinetics of the bcc to hcp phase transition in single crystal iron when ramp-compressed along the [001] crystallographic direction. Samples containing up to 28 million atoms were simulated using the LAMMPS molecular dynamics code [19], where the interactions between atoms were modeled through the embedded atom model formalism [20, 21]. The iron model was the modified version of the Ackland potential

[11], which was successfully used in the past to account for both plasticity and phase transition in iron [11, 12, 22].

Both defect-free and defective initial conditions have been investigated, where the defects were introduced within the sample in the form of microvoids of  $5 a_0$  radius, where  $a_0$  is the lattice constant, regularly spaced by  $100 a_0$  along the wave propagation direction  $z$ . Samples were first thermalized to 50 K and then compressed by driving an effective infinite-mass wall piston with an imposed velocity  $v$  along the  $z$ -direction while periodic boundary conditions were used for the transverse directions. The ramp compression was realized by linearly increasing the piston velocity from zero to its maximum during 30 ps and then held constant at that maximum until the end of the simulation. Piston maximum velocity ranging from 600 to 1600  $m.s^{-1}$  were investigated, corresponding to compression rates ranging from  $10^8$  to  $10^9 s^{-1}$  comparable with that reported under picosecond-laser dynamic compression [23]. Maximum pressure at the top of the ramp ranges from 31 GPa to 140 GPa.

Local thermodynamic and mechanical properties such as longitudinal pressure  $P_z$ , shear stress, temperature, etc. were evaluated within a spatial planar bin (of  $3 a_0$  width) perpendicular to the wave propagation direction in same manner as in references [14, 15, 17]. Finally, local structural analysis was performed by adaptative Common Neighbor Analysis (CNA), Centrosymmetry and Dislocation Analysis Tool (DXA) as implemented in the OVITO software [24].

### 3 Results and Discussion

Fig. 1 illustrates the response of a defect-free crystal to ramp compression along the [001] direction up to a maximum piston velocity of 600  $m.s^{-1}$ , corresponding to a maximum pressure of 31 GPa. It starts with the propagation of an elastic wave up to a yield strength of about 12 GPa (Fig. 1a). Then, the plastic deformation of the bcc phase proceeds by the nucleation of numerous stacking faults identified to be micro-twins (Fig. 1c). Because the bulk sound speed increases with pressure, the ramp wave above the elastic limit classically steepens during its propagation (Fig. 1a) to form a shock wave after about 50 ps. The shear stress is partially relaxed at the beginning of plastic deformation, but it is observed to increase again upon further compression, up to about 2 GPa (Fig. 1b). This unexpected, post-yield stiffening was evidenced and discussed in more details in previous articles, where it was referred to as a hardening-like effect [14, 15, 16, 17]. It was shown to shift the bcc-hcp transition in iron to very high onset pressures [14], so that the 31 GPa final pressure in the simulation is not enough to initiate this transformation.

Fig. 2 shows the same ramp-loading case for a sample where initial defects were introduced in the form of microvoids. Plastic deformation remains similar to that of the perfect crystal, i.e. mainly dominated by deformation twinning (Fig. 2 d, e). The hardening-like effect is observed with the shear stress increasing again with further compression beyond the yield strength. However, defects now lower the energy barrier of the phase transition and accelerate its kinetics [25, 26]. As a consequence, hcp and fcc phases are observed to nucleate heterogeneously around the microvoids (Fig. 3) at a pressure  $P_{nu}$  (nucleation) of about 25 GPa, much lower than the 100 GPa required in the case of defect-free crystal. The high pressure hcp phase, mixed with some fcc atoms, develops through a two-step process: an initial nucleation regime with slow transformation kinetics followed by a rapid growth regime in which the hcp/bcc phase interface velocity depends on the over-compression,  $\Delta P = P_{peak} - P_{nu}$ .

During the nucleation regime, the bcc and hcp/fcc phases coexist. Because the growth of the hcp

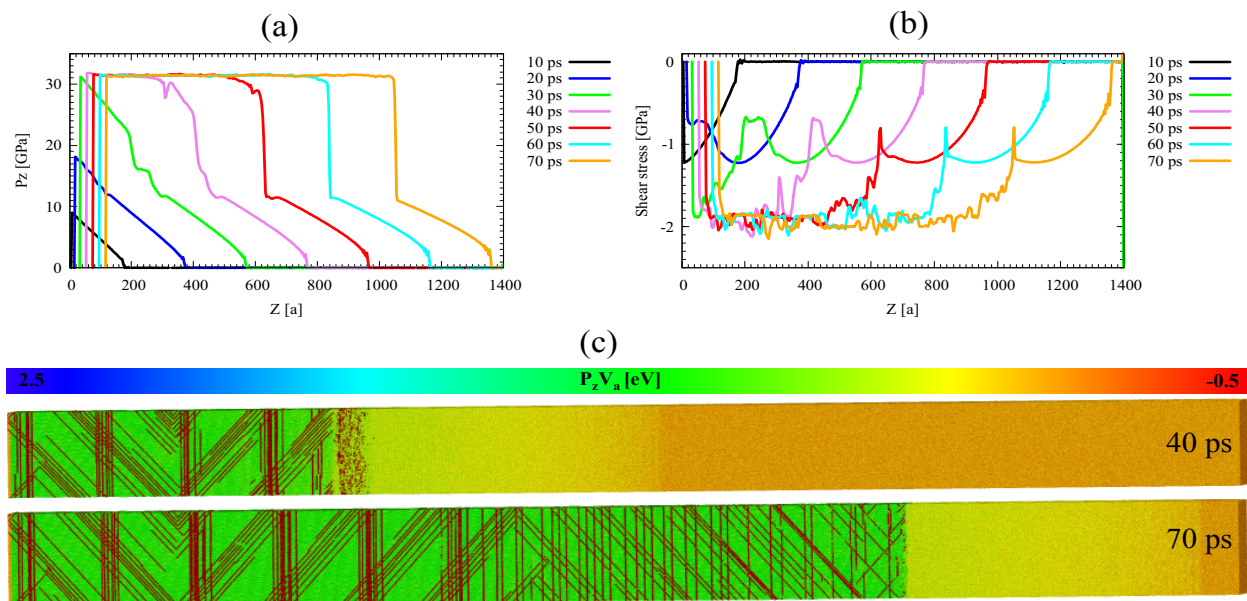


Figure 1: Spatial profiles of the longitudinal pressure  $P_z$  (a) and shear stress (b) for a defect-free single crystal iron ramp compressed to a piston maximum velocity of  $600 \text{ m.s}^{-1}$ . (c) Selected snapshots of atomic configuration showing the wave propagation and micro-twins (brown colored atoms) associated with the plastic deformation. The bcc atoms are colored according to their  $P_z V_a$  value, where  $V_a$  is the atomic volume and  $P_z$ , the pressure component along the wave propagation axis  $z$ . The twins in the bcc phase are colored in brown regardless of the pressure.

phase is limited by its kinetics, its proportion remains very low for a short period during which the macroscopic behavior of the mixture is still essentially that of bcc iron [27]. No effect on wave profiles is observed yet at this stage, where a steady pressure state is maintained behind the ramp wave until about 50 ps (Fig. 2a). Next, the amount of hcp phase becomes sufficient to relax locally the pressure in the mixture, because the bcc-hcp change is associated with a volume reduction. Thereafter, the dynamic behavior results from an interplay between the ramp wave evolution during its propagation and the progressive phase transformation leading to a time dependent bcc/hcp phase boundary velocity [28, 29]. For this low piston velocity of  $600 \text{ m.s}^{-1}$ , the corresponding maximum pressure is about 31 GPa resulting in a small over-compression. Therefore, the bcc to hcp phase transition kinetics is slow (Fig. 2c), with the hcp phase nucleation activated around several microvoids before the onset of a rapid growth regime (see Fig. 3). Due to kinetic effects, the pressure release accompanying the phase transformation becomes more important with increasing simulation time (Fig. 2a). Then, follows a region where bcc iron is converted to almost full hcp phase over some lattice constants. Here, we refer to as hcp/bcc phase boundary this region that separates the almost full hcp phase from the hcp/bcc mixture. Behind this phase boundary, the transition is completed and the hcp iron is compressed to the final steady state. For the maximum piston velocity of  $600 \text{ m.s}^{-1}$ , the velocity of this phase boundary interface is about  $2000 \text{ m.s}^{-1}$  (Fig. 4), so that several nucleation sites are still active up to a simulation time of 80 ps. The pressure relaxation associated with the transition is about 5.5 GPa.

Ahead of the phase transition, the plastic activity in the bcc phase generates twins, which tend to become thicker with time (Fig. 2d and 2e). They survive further compression in this case because the shear stress is locally relaxed (Fig. 2b) by the germination of hcp nuclei around the microvoids. In

fact, the microstructure of the daughter hcp phase behind the transition front is found to be strongly affected by those twins inherited from plastic deformation in the parent phase. Indeed, it contains distinct regions delimited by former twin boundaries (at  $45^\circ$  from the  $z$  direction in Fig. 2d, and normal to that direction in Fig. 2e). Actually, these regions are shown to be twins within the hcp phase, as assessed by the crystal symmetries across the green-colored boundaries in Fig. 5a and 5b. Besides, as previously reported [30], the hcp nuclei are observed to develop more rapidly in the  $(110)$  and  $(\bar{1}\bar{1}0)$  planes than along the perpendicular direction. This anisotropic growth leads to secondary twinning within the hcp phase [3, 31], as illustrated in Fig. 5c. Thus, the microstructure in the hcp phase is conditioned by the plastic activity in the bcc phase, leading to a microstructure composed of twins inside twins as observed for other bcc metals such tantalum [32].

When the piston maximum velocity is increased beyond  $800 \text{ m.s}^{-1}$ , although the micro-twins in the bcc phase still survive, their density becomes very low upon further compression by the P1 wave. Consequently, they are completely annihilated during the phase transition. Note that this effect

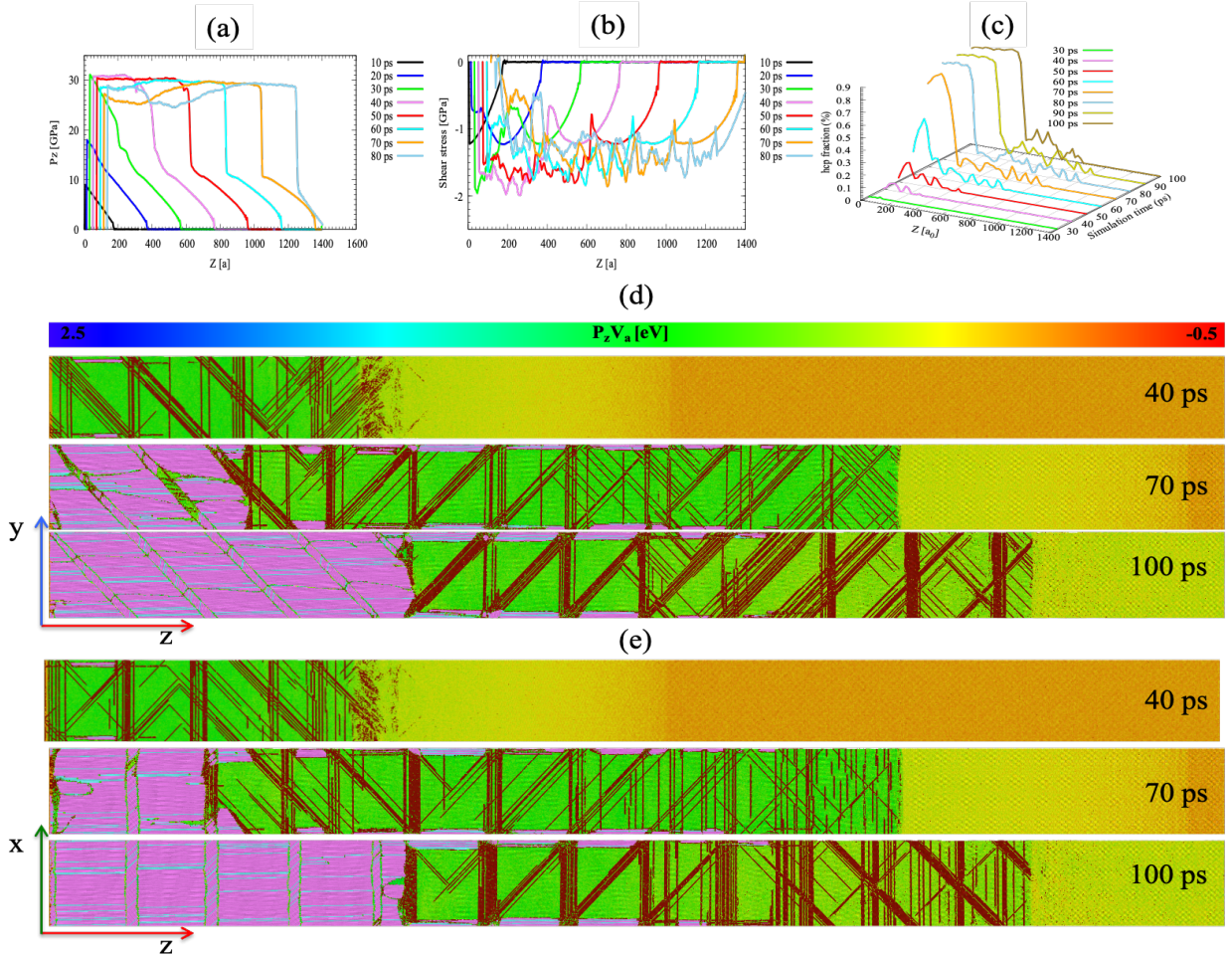


Figure 2: Spatial profiles of the longitudinal pressure  $P_z$  (a), shear stress (b) and hcp phase fraction (c) along the wave propagation axis  $z$  for a defective  $[001]$ -oriented single crystal iron ramp compressed to a piston maximum velocity of  $600 \text{ m.s}^{-1}$  during 30 ps. (d) and (e): selected snapshots of atomic configuration showing the correlation between deformation twinning in the bcc phase (atoms colored in brown) and the microstructure in the hcp phase (atoms colored in violet). Atoms colored in cyan are fcc atoms.

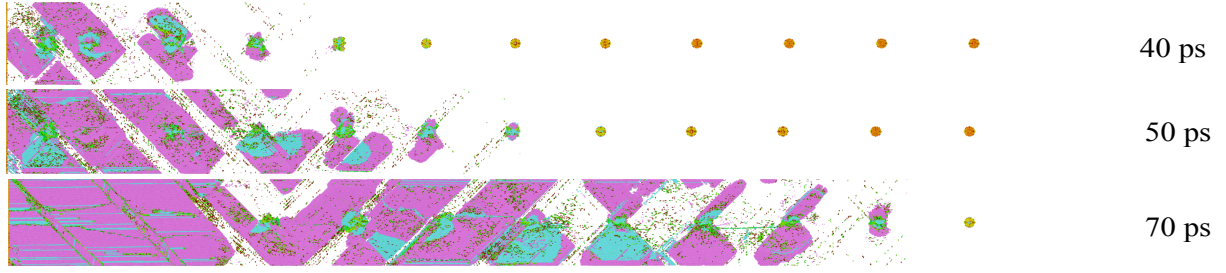


Figure 3: Nucleation and growth of the high pressure hcp phase (violet colored atoms), including some atoms of fcc type (cyan colored atoms), around the initial defects in a defective single crystal iron ramp-compressed to a piston maximum velocity of  $600 \text{ m.s}^{-1}$  (same as Fig. 2d, but without displaying the bcc atoms).

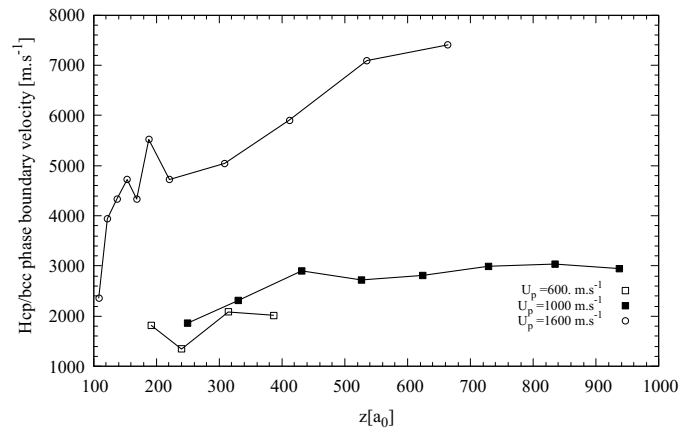


Figure 4: bcc/hcp phase boundary velocity for maximum piston velocities of  $600 \text{ m.s}^{-1}$  (a),  $1000 \text{ m.s}^{-1}$  (b) and  $1600 \text{ m.s}^{-1}$  (c). In this latter case, the phase boundary progressively accelerates during its propagation and overtakes the longitudinal sound speed of about  $6 \text{ km.s}^{-1}$  in iron.

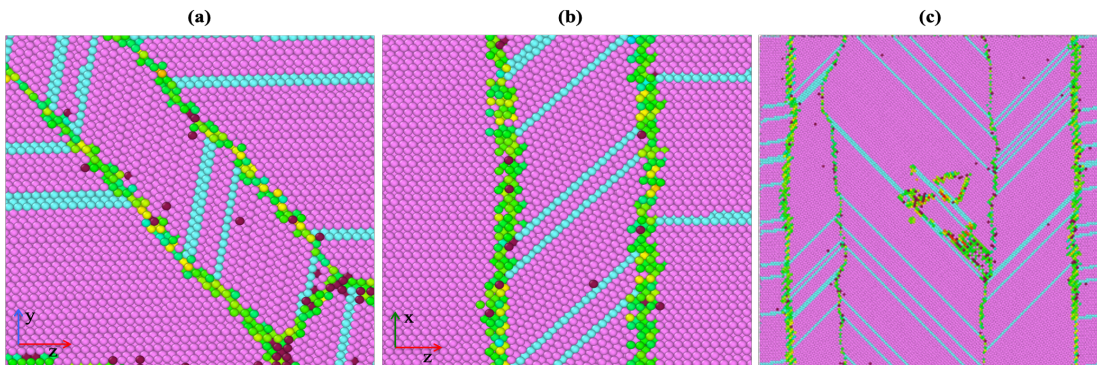


Figure 5: : Atomic configurations in y-z (a) and x-z (b) sections showing the microstructure in the hcp phase with primary twins (region between the two lines of green-colored atoms) issued from the plastic activity in the bcc phase. (c) cross-section perpendicular to the z-axis across the twin of (b) showing secondary twinning activity resulting from the hcp phase nucleation and growth.

depends on the pressure state behind the plastic deformation wave and not on the strain rate, since it is still observed when changing the ramp rise time.

The phase boundary velocity increases with the over-compression in agreement with the classical theory of nucleation and growth [28, 29]. When the piston maximum velocity is increased to  $1000 \text{ m.s}^{-1}$  (Fig. 6) and higher, the pressure profiles show the common three-wave structure, with an elastic precursor followed by the P1 wave compressing the bcc phase up to a plateau, then the P2 wave where the bcc to hcp phase transformation occurs followed by subsequent compression to the final pressure. At early times, the velocity of phase boundary is low (Fig. 4), so that nucleation has time to develop around the microvoids leading to a mixed bcc and hcp/fcc regime behind the P1 wave (Figs. 6c and Fig. 7). A plateau is progressively formed in wave profiles corresponding to the onset of the phase transition. With increasing propagation distance, the pressure at the plateau decreases from 37.1 GPa at 30 ps to 29.2 GPa at 60 ps, while the plateau duration decreases in consistence with experimental observations under nanosecond laser compression [33, 27]. Next, as the kinetics accelerates with the pressure in the ramp, the velocity of the phase boundary increases up to an approximately steady value about  $3000 \text{ m.s}^{-1}$  (Fig. 4). Although, this value is lower than the local sound velocity, the interface progressively engulfs the nucleation region. At late times, the transition occurs through a single sharp front where initial defects which provided nucleation sites facilitating the onset of the transformation do not play this role anymore. Thus, the amplitude of the P1 wave, i.e. the transition onset pressure,

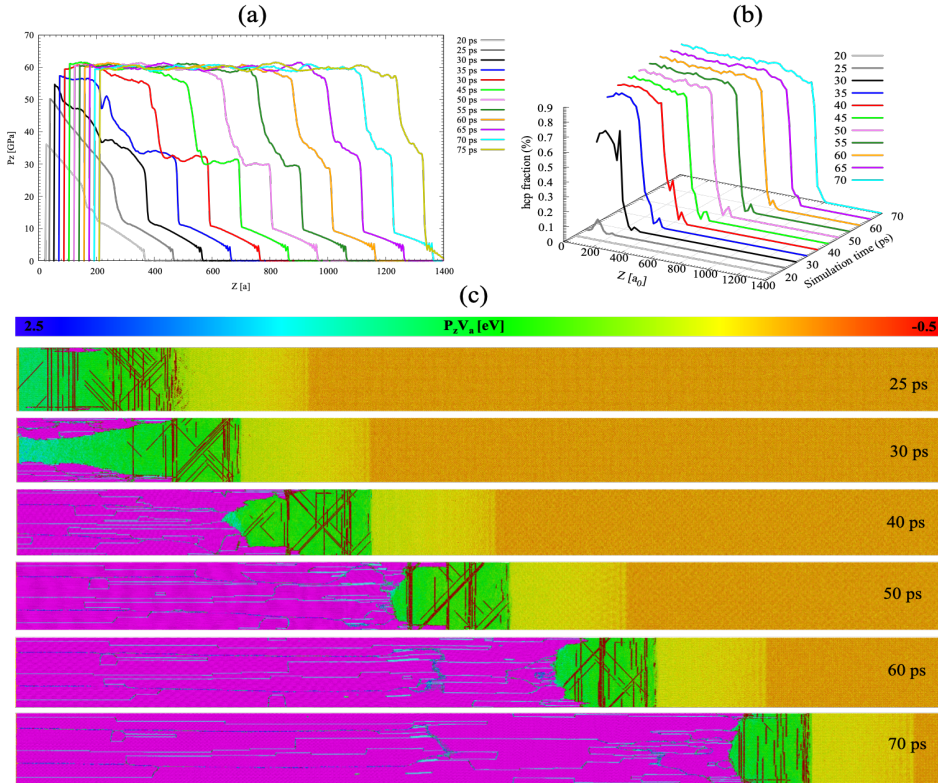


Figure 6: : Spatial profiles of the longitudinal pressure  $P_z$  (a) and hcp phase fraction (b) along the wave propagation axis  $z$  for a defective [001]-oriented single crystal iron when the bcc to phase is overcompressed to a piston maximum velocity of  $1000 \text{ m.s}^{-1}$  during 30 ps. (c) selected snapshots of atomic configuration showing the wave propagation, defects associated with the plastic deformation and local phase structures. The atoms colors are the same as in Fig. 2.

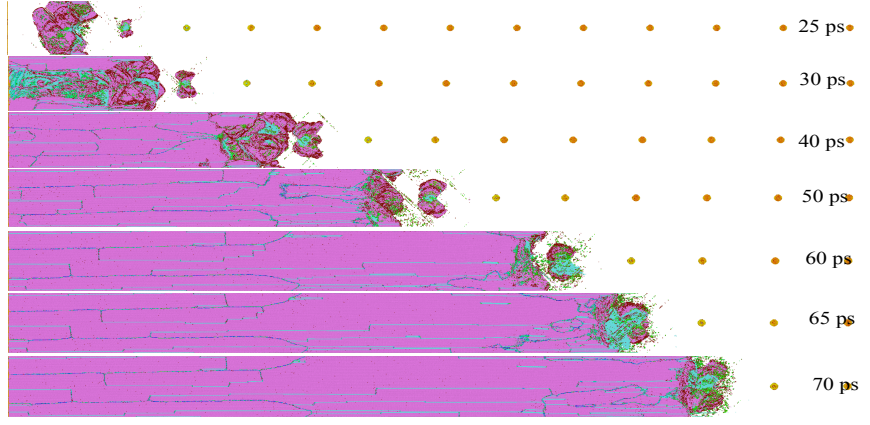


Figure 7: : Nucleation and growth of the high pressure hcp phase (violet colored atoms), including some atoms of fcc type (cyan colored atoms), around the initial defects in a defective single crystal iron when the bcc to hcp phase transition is over-compressed to a piston maximum velocity of  $1000 \text{ m.s}^{-1}$  (same as Fig. 6c, but without displaying the bcc atoms).

is observed to increase (Fig. 6a).

Finally, when highly over-compressed at a piston velocity of  $1600 \text{ m.s}^{-1}$  (Fig. 8), the dynamic

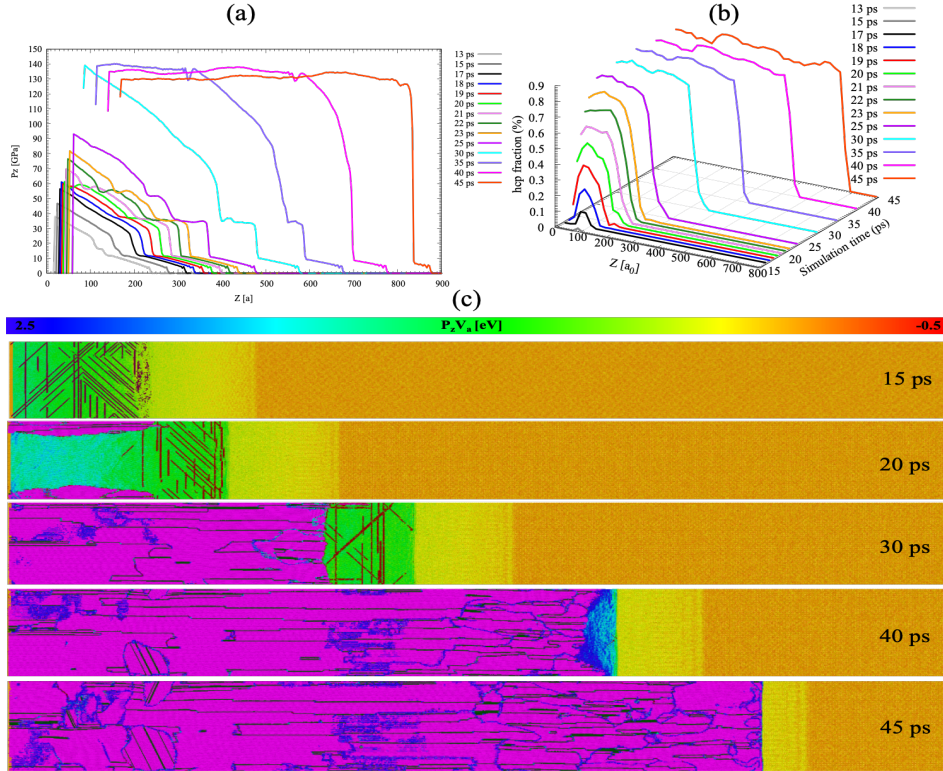


Figure 8: : Spatial profiles of the longitudinal pressure  $P_z$  (a) and hcp phase fraction (b) along the wave propagation axis  $z$  for a defective  $[001]$ -oriented single crystal iron when the bcc to phase is highly over-compressed to a piston maximum velocity of  $1600 \text{ m.s}^{-1}$  during 30 ps. (c) selected snapshots of atomic configuration showing the wave propagation, defects associated with the plastic deformation and local phase structures. The atoms colors are the same as in Fig. 2.

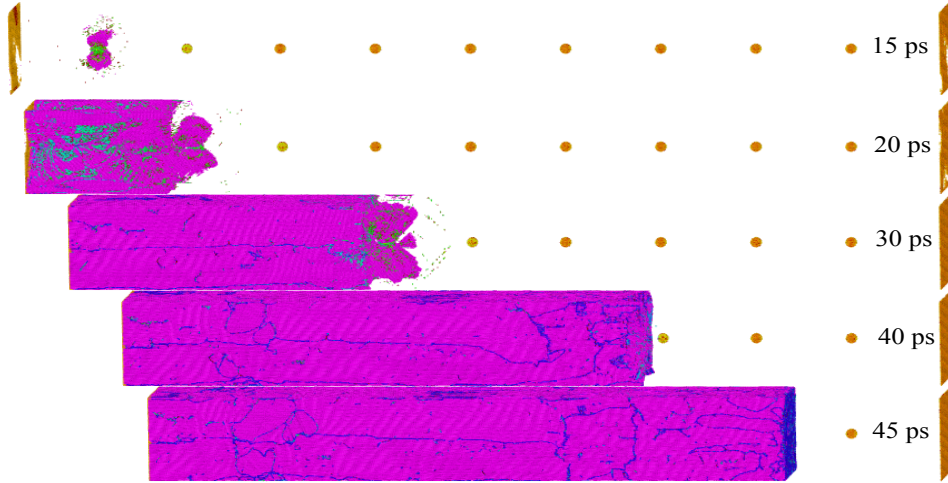


Figure 9: Nucleation and growth of the high pressure hcp phase (violet colored atoms), including some atoms of fcc type (cyan colored atoms), around the initial defects in a defective single crystal iron where the bcc to hcp phase transition is highly over-compressed to a piston maximum velocity of  $1600 \text{ m.s}^{-1}$  (same as Fig. 8 without displaying bcc atoms).

response is initially similar to that of the previous case, although the ramp is steeper (by a factor 1.6). Then, due to the rapid evolution of the pressure in the ramp, the plateau at the onset of the phase transition propagates without any significant pressure relaxation while the phase boundary velocity increases with increasing time, up to becoming supersonic (Fig. 4). The phase transition then becomes almost instantaneous, across a very sharp front now independent on the presence of pre-existing defects (Fig. 9). Along with this transition front, the P2 wave becomes steeper too, due to the increase of sound velocity with pressure, and exhibits a classical evolution into a shock front, which velocity is now higher than that of the P1 wave. In this overdriven regime, the compression consists of a small elastic precursor followed by a single shock front where the bcc phase is instantaneously converted to hcp phase, which is also instantaneously compressed to the final pressure (Figs. 8c and 9). This is consistent with the simple hydrodynamic description of shock wave physics and with experimental observations [34, 35]. All these results are in qualitative agreement with the phenomenological models proposed by Kolmogorov [36] and Avrami [37, 38, 39], where the interface velocity is a function of the over-compression [28].

## 4 Conclusion

Non Equilibrium Molecular dynamics (NEMD) simulations have been used to study the kinetics of the bcc to hcp phase transition in single-crystal iron when ramp compressed along the [001] crystallographic direction in the presence of initial defects. Depending on the ramp maximum pressure, the microstructure in the hcp phase is found to be strongly conditioned by deformation twinning in the bcc phase, as well as by anisotropic growth of hcp nuclei. This leads to secondary twins inside larger twins directly inherited from the plastic activity in the parent phase prior to the transformation. The bcc/hcp phase boundary velocity increases with the over-compression in accordance with classical theories of nucleation and growth. These results provide insight into the mechanisms governing displacive phase transformations and their dynamics. They confirm the good capabilities of the modified Ackland

potential to predict many realistic features of the complex behavior of dynamically compressed iron, and they are expected to be used to improve kinetic models implemented in hydrodynamic codes.

## Acknowledgments

Computations were performed on the supercomputer facilities of the Mésocentre de calcul de Poitou Charentes (France). This work was partially funded by the French Program CNRS-Africa

## References

- [1] R. Harrison, Voter A. F., , and S.-P. Chen. *in Atomistic Simulation of Material*. 1989. pp: 219.
- [2] K. Kadau, T. C. Germann, P. S. Lomdahl, and B. L. Holian. Shock-induced structural phase transformations studied by large-scale molecular-dynamics simulations. *AIP Conf. Proceedings*, 620(1):351–354, 2002.
- [3] K. Kadau, T. C. Germann, P. S. Lomdahl, and B. L. Holian. Atomistic simulations of shock-induced transformations and their orientation dependence in Bcc Fe single crystals. *Phys. Rev. B*, 72:064120, 2005.
- [4] K. Kadau, T. C. Germann, P. S. Lomdahl, R. C. Albers, J. S. Wark, A. Higginbotham, and B. L. Holian. Shockwaves in polycrystalline iron. *Phys. Rev. Lett.*, 98:135701, 2007.
- [5] B. J. Jensen, G. T. Gray, and R. S. Hixson. Direct measurements of the  $\alpha$ - $\epsilon$  transition stress and kinetics for shocked iron. *J. Appl. Phys.*, 105:103502, 2009.
- [6] Jian-Li Shao, Weihua He, Tao Xi, and Jianting Xin. Microscopic insight into the structural transition of single crystal iron under the ramp wave loading. *Computational Materials Science*, 182:109772, 2020.
- [7] James H. Rose, John R. Smith, Francisco Guinea, and John Ferrante. Universal features of the equation of state of metals. *Phys. Rev. B*, 29:2963–2969, Mar 1984.
- [8] Xinlin Cui, Wenjun Zhu, Hongliang He, Xiaoliang Deng, and Yingjun Li. Phase transformation of iron under shock compression: Effects of voids and shear stress. *Phys. Rev. B*, 78:024115, Jul 2008.
- [9] K. Wang, S. Xiao, H. Deng, W. Zhu, and W. Hu. An atomic study on the shock-induced plasticity and phase transition for iron-based single crystals. *Int. J. Plast.*, 59:180 – 198, 2014.
- [10] K. Wang, W. Zhu, S. Xiao, K. Chen, H. Deng, and W. Hu. Coupling between plasticity and phase transition of polycrystalline iron under shock compressions. *Int. J. Plast.*, 71:218 – 236, 2015.
- [11] N. Gunkelmann, E. M. Bringa, K. Kang, G. J. Ackland, C. J. Ruestes, and H. M. Urbassek. Polycrystalline iron under compression: Plasticity and phase transitions. *Phys. Rev. B*, 86:144111, 2012.

- [12] N. Gunkelmann, E. M. Bringa, D. R. Tramontina, C. J. Ruestes, M. J. Suggit, A. Higginbotham, J. S. Wark, and H. M. Urbassek. Shock waves in polycrystalline iron: Plasticity and phase transitions. *Phys. Rev. B*, 89:140102, 2014.
- [13] Hoang-Thien Luu, Ramon J. Ravelo, Martin Rudolph, Eduardo M. Bringa, Timothy C. Germann, David Rafaja, and Nina Gunkelmann. Shock-induced plasticity in nanocrystalline iron: Large-scale molecular dynamics simulations. *Phys. Rev. B*, 102:020102, Jul 2020.
- [14] N. Amadou, T. de Resseguier, A. Dragon, and E. Brambrink. Coupling between plasticity and phase transition in shock- and ramp-compressed single-crystal iron. *Phys. Rev. B*, 98:024104, Jul 2018.
- [15] N. Amadou, T. De Resseguier, A. Dragon, and E. Brambrink. Effects of orientation, lattice defects and temperature on plasticity and phase transition in ramp-compressed single crystal iron. *Comput. Mater. Sci.*, 172:109318, 2020.
- [16] N. Amadou, T. de Resseguier, and A. Dragon. Coupling between plasticity and phase transition in single crystal iron at ultra-high strain rate. *AIP Conference Proceedings*, 2272(1):070001, 11 2020.
- [17] Nourou Amadou, Abdoul Razak Ayouba Abdoulaye, Thibaut De Resseguier, and André Dragon. Strain-rate dependence of plasticity and phase transition in [001]-oriented single-crystal iron. *Crystals*, 13(2):250, 2023.
- [18] B. A. Remington, G. Bazan, J. Belak, E. Bringa, J. D. Colvin, M. J. Edwards, S. G. Glendinning, D. H. Kalantar, M. Kumar, B. F. Lasinski, K. T. Lorenz, J. M. McNaney, S. M. Pollaine, D. Rowley, J. S. Stölken, S. V. Weber, W. G. Wolfer, M. Caturla, D. S. Ivanov, L. V. Zhigilei, B. Kad, M. A. Meyers, M. Schneider, D. D. Meyerhofer, B. Yaakobi, and J. S. Wark. Materials science under extreme conditions of pressure and strain rate. *Metallurgical and Materials Transactions A*, 35(9):2587, Sep 2004.
- [19] S. Plimpton. Fast parallel algorithms for short-range molecular dynamics. *J. Comp. Phys.*, 117:1–19, 1995.
- [20] M. S. Daw and M. I. Baskes. Semiempirical, quantum mechanical calculation of hydrogen embrittlement in metals. *Phys. Rev. Lett.*, 50:1285–1288, 1983.
- [21] S. M. Foiles, M. I. Baskes, and M. S. Daw. Embedded-atom-method functions for the fcc metals Cu, Ag, Au, Ni, Pd, Pt, and their alloys. *Phys. Rev. B*, 33:7983–7991, 1986.
- [22] N. Gunkelmann, D. R. Tramontina, E. M. Bringa, and H. M. Urbassek. Interplay of plasticity and phase transformation in shock wave propagation in nanocrystalline iron. *New J. Phys.*, 16(9):093032, 2014.
- [23] J. C. Crowhurst, B. W. Reed, M. R. Armstrong, H. B. Radousky, J. A. Carter, D. C. Swift, J. M. Zaug, R. W. Minich, N. E. Teslich, and M. Kumar. The  $\alpha - \epsilon$  phase transition in iron at strain rates up to  $10^9 s^{-1}$ . *J. Appl. Phys.*, 115(11):113506, 2014.

- [24] A. Stukowski. Visualization and analysis of atomistic simulation data with OVITO—the open visualization tool. *Modelling and Simulation in Materials Science and Engineering*, 18:015012, 2009.
- [25] J. W. Christian. *The Theory of Transformations in Metals and Alloys*. Elsevier, 2002. pp: 464.
- [26] R. E. Smallman and A. H. W. Ngan. *Modern Physical Metallurgy*. Elsevier, 2014.
- [27] N. Amadou, T. de Resseguier, E. Brambrink, T. Vinci, A. Benuzzi-Mounaix, G. Huser, G. Morard, F. Guyot, K. Miyanishi, N. Ozaki, R. Kodama, and M. Koenig. Kinetics of the iron  $\alpha - \epsilon$  phase transition at high-strain rates: Experiment and model. *Phys. Rev. B*, 93:214108, Jun 2016.
- [28] N. Hamaya, Y. Yamada, J. D. Axe, D. P. Belanger, and S. M. Shapiro. Neutron scattering study of the nucleation and growth process at the pressure-induced first-order phase transformation of RbI. *Phys. Rev. B*, 33:7770–7776, Jun 1986.
- [29] M. Bastea, S. Bastea, and R. Becker. High pressure phase transformation in iron under fast compression. *Appl. Phys. Lett.*, 95:241911, Dec. 2009.
- [30] N. Amadou, T. de Resseguier, and A. Dragon. Influence of point defects and grain boundaries on plasticity and phase transition in uniaxially-compressed iron. *Computational Condensed Matter*, 27:e00560, 2021.
- [31] N. Amadou and T. de Resseguier. Phase transformations and plasticity in single-crystal iron from shock compression to spall fracture. *Phys. Rev. B*, 108:174109, Nov 2023.
- [32] L. A. Zepeda-Ruiz, A. Stukowski, T. Oettel, and V. V. Bulatov. Probing the limits of metal plasticity with molecular dynamics simulations. *Nature*, 550:492, 2017.
- [33] R. F. Smith, J. H. Eggert, D. C. Swift, J. Wang, T. S. Duffy, D. G. Braun, R. E. Rudd, D. B. Reisman, J.-P. Davis, M. D. Knudson, and G. W. Collins. Time-dependence of the alpha to epsilon phase transformation in iron. *J. Appl. Phys.*, 114(22):223507, 2013.
- [34] N. Amadou, Erik Brambrink, Alessandra Benuzzi-Mounaix, T. Vinci, Thibaut de Resseguier, S. Mazevet, G. Morard, F. Guyot, Norimasa Ozaki, Kohei Miyanishi, and M. Koenig. Laser-driven quasi-isentropic compression experiments and numerical studies of the iron alpha-epsilon transition in the context of planetology. *AIP Conference Proceedings*, 1426(1):1525–1528, 03 2012.
- [35] N. Amadou, E. Brambrink, A. Benuzzi-Mounaix, G. Huser, F. Guyot, S. Mazevet, G. Morard, T. de Resseguier, T. Vinci, K. Myanishi, N. Ozaki, R. Kodama, T. Boehly, O. Henry, D. Raffestin, and M. Koenig. Direct laser-driven ramp compression studies of iron: A first step toward the reproduction of planetary core conditions. *High Energy Density Physics*, 9(2):243–246, 2013.
- [36] Bernd A. Berg and Santosh Dubey. Finite volume kolmogorov-johnson-mehl-avrami theory. *Phys. Rev. Lett.*, 100:165702, Apr 2008.
- [37] Melvin Avrami. Kinetics of Phase Change. I General Theory. *The Journal of Chemical Physics*, 7(12):1103–1112, 12 1939.

- [38] Melvin Avrami. Kinetics of Phase Change. II Transformation-Time Relations for Random Distribution of Nuclei. *The Journal of Chemical Physics*, 8(2):212–224, 02 1940.
- [39] Melvin Avrami. Granulation, Phase Change, and Microstructure Kinetics of Phase Change. III. *The Journal of Chemical Physics*, 9(2):177–184, 02 1941.